Materials Advances

ROYAL SOCIETY OF CHEMISTRY

PAPER

View Article Online
View Journal | View Issue

Cite this: *Mater. Adv.*, 2023, 4, 2457

Strong and tough octyl enamine-grafted polyvinyl alcohol with programmable shape deformation *via* simple soaking treatment†

Xiaomin Chen,[ab] Youwei Ma,[b] Yuhong Qiao,[ab] Wenyao Guo,[a] Yulin Min,[a] Jinchen Fan *[ac] and Zixing Shi *[b]

Received 21st April 2023,
Accepted 2nd May 2023

DOI: 10.1039/d3ma00187c

rsc.li/materials-advances

Devising shape-configurable polymeric materials with high strength, large ductility, and great toughness is highly challenging and ever-increasingly desired. Here, octyl enamine-grafted polyvinyl alcohol with a sheath–core structure (AAPVA$_x$–OA) was prepared by soaking treatment of acetoacetylated polyvinyl alcohol (AAPVA$_x$) in the presence of octylamine (OA). The octyl enamine-grafted sheath is stiffer than the ungrafted core in AAPVA$_x$–OA possibly due to the strong hydrogen bonding. The mechanical properties of AAPVA$_x$–OA are superior to those of AAPVA$_x$–JOA, synthesized by solution casting of the blends of AAPVA$_x$ and OA, since the hard-sheath–soft-core structure contributes to the stress transfer and energy dissipation of AAPVA$_x$–OA upon stretching. Moreover, AAPVA$_x$ previously printed with octyl enamines in the predetermined areas can be programmed into the corresponding shapes in the presence of water. We believe that this work provides a new perspective for designing polymeric materials with high mechanical properties and shape-configuration ability using a simple soaking strategy, which can be implemented in other cases as well.

1. Introduction

Polymeric materials are becoming increasingly indispensable in our daily life owing to their light weight, good chemical resistance, and excellent mechanical properties.[1] Considering the sustainable development of modern society and the increasing demand for advanced polymeric materials, it is urgent to design and manufacture polymeric materials with high strength, large ductility and great toughness. In most materials, however, strength and ductility are regulated by different mechanical mechanisms, so they are generally considered mutually exclusive.[2,3] However, in recent years, inspired by biological materials such as nacre,[4–6] human bone,[7] natural bamboo,[8–10] and lobster cuticle,[11–13] some super strong polymeric composites have been prepared based on their multi-scale hierarchical structure. However, most of them are stiff and yet brittle, and the fracture strain is generally less than 100%.[14] This is mainly attributed to that it is extremely challenging to balance a good hierarchy with excellent mechanical properties. In addition, traditional methods for designing and manufacturing new materials usually produce materials with a relatively uniform composition and microstructure, which seldom integrate high strength, large ductility, and functionality into one material.[15] Therefore, so far, devising functional polymeric materials with high tensile strength and large fracture strain has been a scientific challenge and also an opportunity for researchers.

Acetoacetylated polyvinyl alcohol (AAPVA) synthesized by grafting polyvinyl alcohol (PVA) with acetoacetyl groups has been widely used in textile, construction, medicine, electronics and other industries due to its versatile reactivity.[16] The acetoacetyl groups are able to react with amines to form enamine bonds at room temperature in the absence of catalysts.[16–21] Therefore, the introduction of acetoacetyl groups makes AAPVA highly reactive,[22] and upon further reaction different functions can be introduced to AAPVA by the treatment of various functional amines, which would broaden the applications of AAPVA.[16] The solution blending strategy (such as a one-pot method) adopted in the preparation of traditional polymeric materials usually creates a homogeneous structure, once the chemical composition sets, which

[a] *Shanghai Key Laboratory of Materials Protection and Advanced Materials in Electric Power, College of Environmental and Chemical Engineering, Shanghai University of Electric Power, Shanghai, 200090, China. E-mail: jcfan@usst.edu.cn*
[b] *School of Chemistry & Chemical Engineering, State Key Laboratory for Metal Matrix Composite Materials, Shanghai Jiao Tong University, Shanghai 200240, China. E-mail: zxshi@sjtu.edu.cn*
[c] *School of Materials and Chemistry, University of Shanghai for Science and Technology, Shanghai, 200093, China*

† Electronic supplementary information (ESI) available. See DOI: https://doi.org/10.1039/d3ma00187c

then becomes difficult to improve the mechanical properties and functions of the polymers. Recently, our group found that the polymeric film materials prepared using a soaking strategy not only retained the original characteristics of the constituent materials, but also showed more superior performance in the mechanical and other functional properties.[23] The soaking strategy here refers to the process of immersing a prefabricated polymeric film into a liquid or printing the specific area of the film using a modification reagent. When the film material was immersed in a liquid modification reagent, the outer layer of the film immediately contacted and reacted with the soaking liquid, thus becoming denser.[24–27] Then, the denser structure could delay or inhibit further penetration of the liquid inside, thus forming a gradient structure. This film with a gradient heterogeneous structure in its cross-section showed high strength and ductility simultaneously upon stretching. Moreover, a modification reagent was also introduced to the specific areas of the film through printing, and created some unique structures on the surface of the film. Such a structured surface imparted the films with some unique functions, such as shape memory capability, ultraviolet shielding, and fluorescence characteristics.[23] Therefore, multifunctional polymeric materials with excellent mechanical properties can be realized using simple soaking strategies.

In this work, we used a soaking strategy to prepare octyl enamine-grafted polyvinyl alcohol with a sheath–core structure (AAPVA$_x$–OA) by first grafting PVA with the acetoacetyl group followed by the soaking treatment of octylamine. The octyl enamine-grafted PVA with a homogeneous structure (AAPVA$_x$–JOA) was also synthesized by blending acetoacetylated polyvinyl alcohol (AAPVA$_x$) with octylamine. Comparing the two kinds of polymer films, AAPVA$_x$–OA had higher strength and ductility than AAPVA$_x$–JOA. We attributed such superior mechanical properties of AAPVA$_x$–OA to the soaking strategy induced sheath–core structure and the abundant hydrogen bonds, which contribute to the stress transfer and energy dissipation of the film material upon stretching. In addition, on account of the incorporation of octyl groups on the outer layer of AAPVA$_x$–OA, the outer layer becomes hydrophobic and the inner side is still hydrophilic, which makes AAPVA$_x$–OA water responsive. By printing AAPVA$_x$ with octylamine in different areas, the resultant AAPVA$_x$–OA can be configured into different shapes by the treatment of water.

2. Experimental sections

2.1. Materials

Octylamine (OA) and *tert*-butyl acetoacetate (*t*-BAA) (95%) were supplied by Shanghai Titan Scientific Co., Ltd. Poly (vinyl alcohol) (PVA, 1799) was supplied by Shanghai Macklin Biochemical Co., Ltd. All reagents were of analytical grade and used without further purification. Deionized water was used in all cases.

2.2. Preparation of the modified polymeric (AAPVA$_x$) and AAPVA$_x$ films

AAPVA$_X$ (x refers to the mole percentage of *t*-BAA to PVA including 20, 40 and 60) was synthesized and AAPVA$_{40}$ was used as a typical example for description. In general, 5 g of PVA was dispersed in 50 mL of DMSO, and the mixture was heated at 80 °C until the PVA was dissolved completely. Then, the mixture solution was heated to 110 °C, and 6.47 g of *t*-BAA was added dropwise under the protection of nitrogen and stirred for 3 h. After the reaction completed, the products were precipitated and washed with ethanol several times. The washed products were dried at 80 °C for further usage. Similarly, AAPVA$_{20}$ and AAPVA$_{60}$ were synthesized by changing the amount of *t*-BAA. In addition, the AAPVA$_x$ film was fabricated *via* evaporation of the AAPVA$_x$ solution (10 wt%), and was about 260 μm in thickness.

2.3. Soaking strategy to prepare AAPVA$_x$–OA films

The AAPVA$_{40}$ film was used as a typical example to illustrate the soaking modification process in detail. Firstly, 425 mg of octylamine (the molar ratio of octylamine to the acetoacetyl group is 1 : 1) was dissolved in 66.6 mL of toluene. Then, the AAPVA$_{40}$ film (1.0 g) was added into the mixture and kept stirring at room temperature for 12 h. After modification, the film sample was washed with ethanol and toluene to remove the physically adsorbed amino compounds on the surface of the film. Finally, the AAPVA$_{40}$–OA film was obtained by drying at 80 °C for 24 h. Notably, the AAPVA$_{20}$–OA and AAPVA$_{60}$–OA films were also prepared with OA, using a preparation process similar to that of the AAPVA$_{40}$–OA film.

2.4. Blending strategy to prepare AAPVA$_x$–JOA films

To achieve the same grafting ratio of AAPVA$_x$–JOA and AAPVA$_x$–OA, the grafting ratio of the soaking strategy was first determined using a weighing method and was used as the reaction ratio of the blending strategy. AAPVA$_{40}$–JOA was used as an example, and the grafting ratio of the soaking strategy was 0.7. Hence, the molar ratio of octylamine to the acetoacetyl group was 1 : 0.7. To be specific, 1 g of AAPVA$_{40}$ was dissolved in dry 10 mL of DMSO and 298 mg of octylamine dissolved in 5 mL of toluene was added dropwise at room temperature with stirring for 3 h. Then, the obtained solution was cast onto the PTFE mold and kept undisturbed at 80 °C for 72 h to obtain a homogeneous film denoted as AAPVA$_{40}$–JOA. Similarly, the AAPVA$_{20}$–JOA and AAPVA$_{60}$–JOA films were prepared by changing the amount of octylamine using a blending strategy.

2.5. Instruments and characterization

Nuclear magnetic resonance spectroscopy (NMR) was carried out using an AVANCE III HD 500 spectrometer (Bruker Bio Spin Corp.). DMSO-d_6 was used as a solvent and TMS was used as an internal standard at room temperature. Fourier transform infrared spectroscopy (FT-IR) was performed using a PerkinElmer Spectrum100 FTIR spectrometer (UK) with a diamond ATR probe on pressed thin transparent disks of the sample mixed

with KBr. Thermogravimetric analysis (TGA) tests were conducted using a Q5000IR analyzer. The heating rate was 20 °C min^{-1} from room temperature to 800 °C under a flowing N_2 atmosphere. Differential scanning calorimetry (DSC, Q2000, TA Instruments, USA) was performed to test the thermal behavior of materials. The test temperature ranged from 40 °C to 250 °C, the heating rate was 20 °C min^{-1}, and the cooling rate was 5 °C min^{-1}. In order to eliminate thermal history before data were recorded, all samples were first processed at the same warming and cooling rates, and the second warming data were recorded. X-Ray Diffraction (XRD) analysis was performed with Cu Kα radiation (λ = 1.5406 Å) at a generator voltage of 40 kV and a generator current of 200 mA (Philips PW1800, Netherland). The analysis was conducted from 5 to 60° at a scanning rate of 4° min^{-1}. Laser scanning confocal microscope (LSCM, LEXT OLS4100, Olympus, Japan) was used to observe the cross-section morphology of the films. Ultraviolet-visible spectrophotometer (UV-vis, TU-1901, Persee, China) was used to record the transmittance spectra of the films in the wavelength range of 400–800 nm.

2.6. Mechanical testing

The tensile strengths of the $AAPVA_x$, $AAPVA_x$–OA and $AAPVA_x$–JOA films were characterized by tensile testing, which was performed using a universal testing machine (INSTRON 3365, USA) at a tensile rate of 100 mm min^{-1} and an ambient temperature of 25 °C. The film sample was cut into a standard dumbbell sample according to the GB/T528 standard (the length of the film was 50 mm and the width of the test part was 4 mm). In all mechanical measurements, three splines were tested in parallel for each film to obtain reliable values.

Tensile toughness (τ) can be calculated by integrating the area under the stress–strain line using eqn (1).

$$\tau = \sum_{i=0}^{i=\varepsilon} \sigma \varepsilon_i \quad (1)$$

Young's modulus (E) is the ratio of the stress and strain of a material under elastic deformation, as shown in eqn (2)

$$E = \frac{\sigma}{\varepsilon} \quad (2)$$

where E represents Young's modulus, σ represents the tensile stress, and ε represents the tensile strain.

2.7. Swelling testing

The deionized water swelling rates of the $AAPVA_{40}$ and $AAPVA_{40}$–OA films were determined by gravimetry. The test temperature was set as 25 °C. A pre-weighed film (2 × 2 cm) was soaked in 40 mL of deionized water for 72 h. Then, the film was taken out from the water at intervals of 12 h or 24 h each time and weighed after removing surface liquid using a blotting paper. The swelling rate can be calculated by the following eqn (3).

$$\text{Swelling rate}(\%) = \frac{m_{\text{instant}} - m_{\text{initial}}}{m_{\text{initial}}} \times 100\%, \quad (3)$$

where m_{instant} is the immediate weight of the expansion film when it is soaked in water, and m_{initial} is the weight under the initial dry state.

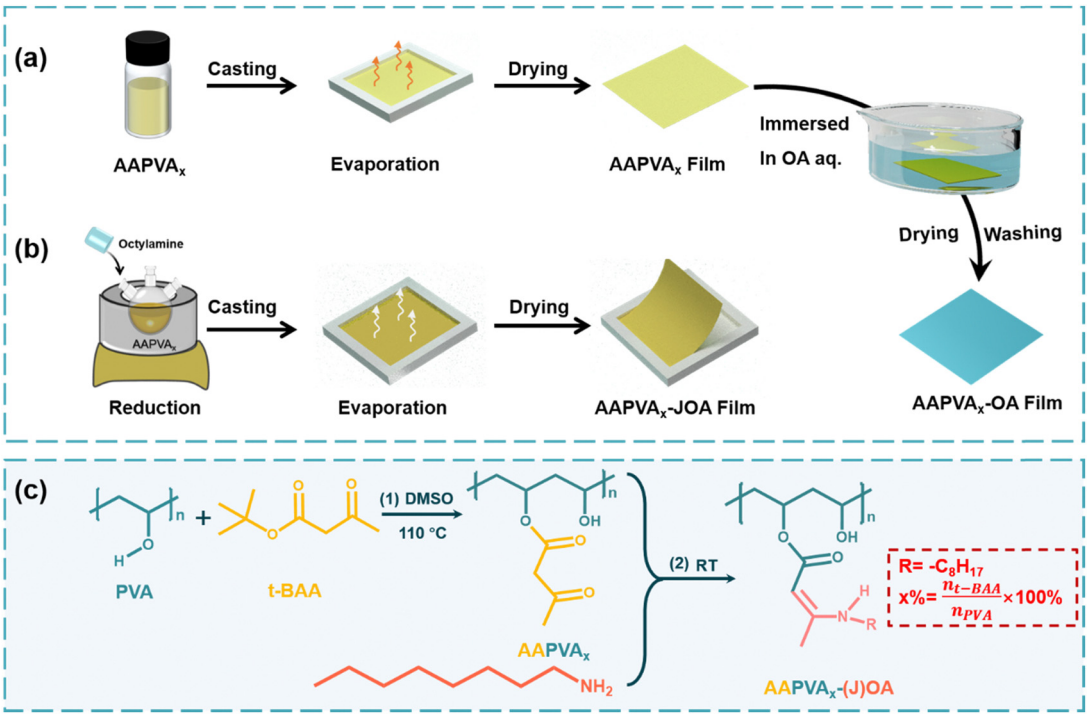

Fig. 1 Schematic illustration of the preparation of $AAPVA_x$–OA by the soaking treatment of $AAPVA_x$ with octylamine (a) and $AAPVA_x$–JOA synthesized by blending $AAPVA_x$ with octylamine (b). Synthesis mechanism of $AAPVA_x$–(J)OA by first grafting PVA with *t*-BAA at 110 °C followed by reacting with octylamine at room temperature (c).

3. Results and discussion

3.1. Synthesis of the characterization of AAPVA$_x$–(J)OA

As a proof of concept, first we fabricated two kinds of film samples. One was synthesized by the soaking treatment of acetoacetylated polyvinyl alcohol (AAPVA$_x$) with octylamine (OA) followed by washing and vacuum drying, which we labeled as AAPVA$_x$–OA (a synthesis scheme in Fig. 1a). The other was prepared by direct solution casting of the blends of AAPVA$_x$ and OA followed by thermal treatment at 80 °C for 72 h, labeled as AAPVA$_x$–JOA (a synthesis scheme in Fig. 1b). Thereinto, AAPVA$_x$ was synthesized by transesterification of PVA with *tert*-butyl acetoacetate (*t*-BAA) under thermal treatment (synthesis in Fig. S1, ESI†). *x* refers to the feeding ratio of *t*-BAA to PVA including 20 mol%, 40 mol%, and 60 mol%. It is not specifically mentioned later that *x* generally represents 40 mol%. The specific synthesis mechanism is illustrated in Fig. 1c, and includes the grafting of PVA with *t*-BAA at 110 °C to produce AAPVA$_x$ and the reaction of AAPVA$_x$ with OA for AAPVA$_x$–(J)OA at room temperature.

The appearance of the characteristic peaks at 1710 and 1730 cm^{-1} assigned to the acetoacetyl groups in the Fourier transform infrared (FT-IR) spectra of AAPVA$_x$ indicates the successful attachment of the acetoacetyl groups on PVA after the reaction with *t*-BAA (Fig. S2, ESI†).[28–30] Meanwhile, the chemical shifts at δ = 2.2 and 3.6 ppm of the acetoacetyl groups emerge in the ^{1}H NMR spectra of AAPVA$_x$, also supporting the formation of AAPVA$_x$ (Fig. S3, ESI†). Upon increasing the value of *x*, the characteristic peaks or chemical shifts increase in the FT-IR spectra (Fig. S2, ESI†) or ^{1}H NMR spectra (Fig. S3, ESI†) of AAPVA$_x$, respectively, indicating the increased grafting ratio as the feeding ratio increases. After the soaking treatment or direct blending with OA at room temperature, the characteristic peaks of the acetoacetyl groups at 1710 and 1730 cm^{-1} weaken, and the new peaks at 1605 and 1650 cm^{-1} assigned to the enamine motif appear in the FT-IR spectra of AAPVA$_x$–OA and AAPVA$_x$–JOA (Fig. 2a), which suggests the reaction of the acetoacetyl groups and OA to produce AAPVA$_x$–(J)OA.

Next, we investigated the thermal properties of AAPVA$_x$–(J)OA by thermogravimetric analysis (TGA) and differential scanning calorimetry (DSC). The TGA curves show that the introduction of octyl groups does not impact the thermal decomposing temperature of AAPVA$_{40}$ at 200 °C to a significant extent (Fig. 2c). While for the glass transition temperature (T_g)

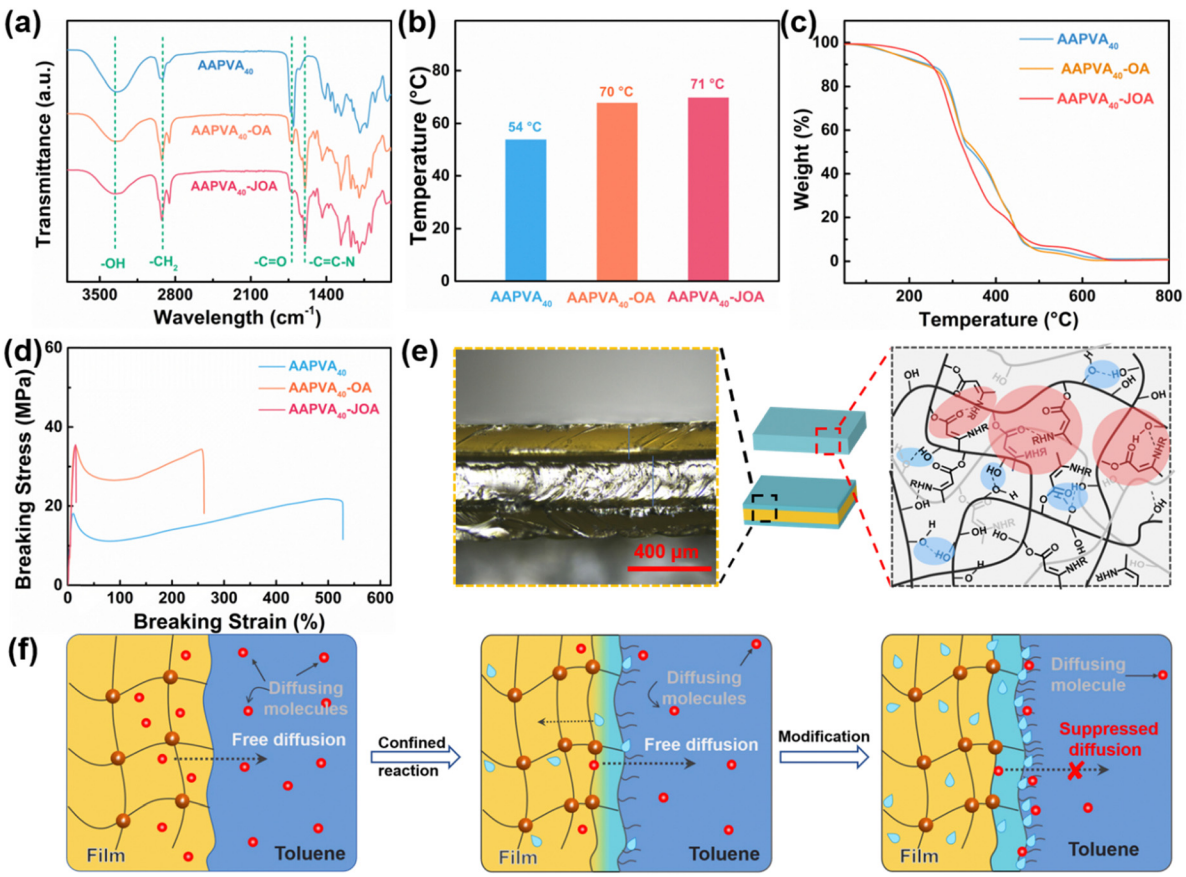

Fig. 2 Characterization and properties of the AAPVA$_{40}$, AAPVA$_{40}$–OA and AAPVA$_{40}$–JOA films. (a) Fourier transform infrared spectra (FT-IR). (b) Comparison of the glass transition temperatures (T_g). (c) Thermal stability of TGA curves and (d) typical stress–strain curves. (e) LSCM images of the cross-sections of AAPVA$_{40}$–OA (left) and the schematic structure of the AAPVA$_x$–JOA films (right) (scale bar: 400 μm). (f) Schematic illustration of the potential forming mechanism of the sheath–core structure in AAPVA$_x$–OA (red dots: octylamines; brown dots: hydrogen bonds; blue dots: water).

measured by DSC (Fig. 2b), it is 51 °C for $AAPVA_{40}$ and after the reaction with octylamine by either the soaking or the blending method, T_g increases to 70 °C for $AAPVA_{40}$–OA or 71 °C for $AAPVA_{40}$–JOA. Moreover, $AAPVA_{40}$ is semicrystalline with an endothermic peak at 137 °C, and the endothermic peak disappears in the DSC curves of $AAPVA_{40}$–(J)OA, indicating an amorphous structure for $AAPVA_{40}$–JOA in the temperature investigated (80–240 °C) (Fig. S4, ESI†). However, $AAPVA_{40}$–OA is a semicrystalline structure. The reason for the disappearance of the melting peak of $AAPVA_{40}$–OA is that the enamine bond is exchanged during the heating process during the DSC test, and the internal $AAPVA_{40}$ is also reacted. The X-ray diffraction (XRD) curve further confirms that $AAPVA_{40}$–OA remains a semicrystalline polymer (Fig. S5, ESI†). After octyl-grafting, the diffraction peaks (2θ = 20°) are weaker and wider, indicating that the crystallinity of $AAPVA_{40}$–OA is significantly lower than that of $AAPVA_{40}$. This may be attributed to the addition of octyl groups, which disturbed the hydrogen bond of the $AAPVA_{40}$ chain. The results reveal that the grafting of octyl groups of $AAPVA_x$–JOA disrupts the crystallization behavior of $AAPVA_x$ possibly due to the hydrophobic octyl impeding the stacking of the hydrophilic polymer chains of $AAPVA_x$. All $AAPVA_x$–OA display a semicrystalline structure, which is attributed to the semicrystalline structure in the soft core of $AAPVA_x$–OA.

Although the chemical compositions of $AAPVA_{40}$–JOA and $AAPVA_{40}$–OA are same, both relying on the reaction between $AAPVA_{40}$ and OA, it is worth mentioning that the mechanical properties of $AAPVA_{40}$–(J)OA are quite distinct. As shown in Fig. 2d, $AAPVA_{40}$ displays a typical behavior of semicrystalline polymers, with an initial elastic regime, yield points at 10% strain. After reacting with OA through simple blending, the resultant $AAPVA_{40}$–JOA does not show a yield regime and becomes brittle. The breaking strength distinctly increases to 35 MPa for $AAPVA_{40}$–JOA from 18 MPa of $AAPVA_{40}$ while the breaking strain decreases to 24% from 528% of $AAPVA_{40}$. We attribute such a difference to the abundant hydrogen bond interaction between enamine and hydroxyls (or carbonyl groups) in $AAPVA_{40}$–JOA (Fig. 2e, right).[31] Compared to $AAPVA_{40}$–JOA, the breaking strength of $AAPVA_{40}$–OA (synthesized by the soaking treatment of $AAPVA_{40}$ with OA) is almost equal to that of $AAPVA_{40}$–JOA (35 MPa *vs.* 35 MPa), but the breaking strain distinctly falls to 20% of $AAPVA_{40}$–JOA from 260% of $AAPVA_{40}$–OA. The decrease in the breaking strain results from the different preparation process for $AAPVA_{40}$–JOA and $AAPVA_{40}$–OA. In

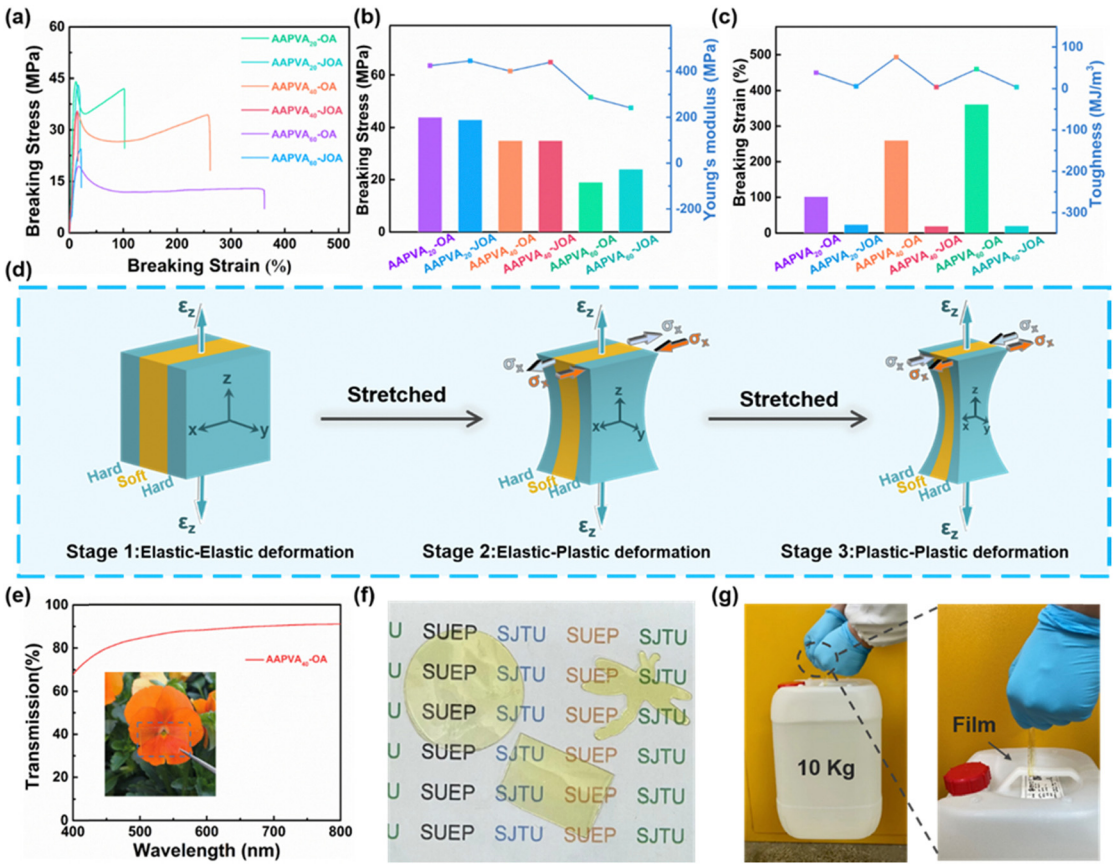

Fig. 3 The mechanical properties of films. (a) Tensile stress–strain curves. (b) Comparison of the tensile strength and Young's modulus. (c) Strain at break and toughness of various film samples. (d) Schematic representation of the mechanically toughening mechanism of $AAPVA_x$–OA films during stretching. (e) UV-vis spectrum and photograph of the $AAPVA_{40}$–OA film (film thickness ≈260 μm). (f) Digital pictures of $AAPVA_{40}$–OA films, showing the excellent tailoring performance. (g) The $AAPVA_{40}$–OA film lifting up a bucket of 10 kg in weight.

the soaking strategy to prepare the $AAPVA_{40}$–OA film, octylamines gradually penetrate and diffuse into $AAPVA_{40}$ (Fig. 2f, left), in which the amines continuously react with the acetoacetyl groups of $AAPVA_{40}$, producing water molecules and an enamine-enriched layer (Fig. 2f, middle). As the diffusion and reaction continue, the generated water will prevent the further diffusion of octylamines into $AAPVA_{40}$, and suppress the reaction between $AAPVA_{40}$ and octylamines (Fig. 2f, right).[32] Such a layer with a thickness of 48 μm on each side of the cross-section of $AAPVA_{40}$–OA can be clearly observed using a laser scanning confocal microscope (LSCM) (Fig. 2e left). By contrast, the LSCM image of the cross-section of $AAPVA_{40}$–JOA shows a homogenous structure. The synergy of the hard sheath layer and the soft core in $AAPVA_{40}$–OA allows transferring the stress and dissipating the energy upon stretching, which contributes the high breaking stress of $AAPVA_{40}$–OA without scarifying its ductility too much, not like that in $AAPVA_{40}$–JOA whose ductility is severely damaged.

3.2. Mechanical properties of $AAPVA_x$–(J)OA

The mechanical properties of $AAPVA_x$–(J)OA with different grafting ratios were further explored by tensile testing, and a comparison among them was made. All $AAPVA_x$–OA (x = 20, 40, 60) display a tensile behavior of semicrystalline polymers, with an initial elastic regime, yield points at 12–19% strain (Fig. 3a), which is attributed to the semicrystalline structure in the soft core of $AAPVA_x$–OA, as revealed by XRD and DSC results (Fig. S5, ESI†). By contrast, $AAPVA_x$–JOA (x = 20, 40, 60) is brittle and fracture at a small strain of 20–24% (Fig. 3a and b). The grafting ratio, *i.e.*, the value of x, has an obvious impact on the mechanical properties of $AAPVA_x$–(J)OA. As x increases, the breaking strain increases clearly from 102% for $AAPVA_{20}$–OA to 260% for $AAPVA_{40}$–OA, then to 362% for $AAPVA_{60}$–OA while the breaking stress gradually decreases from 44 MPa, to 35 MPa, then to 19 MPa accordingly. The same trend is observed in $AAPVA_x$–JOA as well. With the increased x, the breaking stress of $AAPVA_{20}$–JOA constantly reduces from 43 MPa to 35 MPa of $AAPVA_{40}$–JOA, then to 24 MPa of $AAPVA_{60}$–JOA accompanied by its breaking strain maintaining below 30% (24%, 20%, and 21%). The results are possibly due to the high grafting of octyl groups and acetoacetyl groups disturbing the regular structure of PVA.

When comparing the mechanical properties of $AAPVA_x$–OA and $AAPVA_x$–JOA, we see some versatile trends. The breaking stress and Young's modulus of $AAPVA_x$–JOA are at the same level to that of each counterpart of $AAPVA_x$–OA, but the breaking strain and toughness are significantly reduced (Fig. 3b and c). For example, the breaking stress and Young's modulus of $AAPVA_{20}$–JOA are 43 MPa and 445 MPa, respectively, which are almost same to that of $AAPVA_{20}$–OA. The breaking strain and toughness of $AAPVA_{20}$–JOA are 24% and 5.5 MJ m^{-3}, respectively, which are 3.3 times and 5.9 times lower than those of $AAPVA_{20}$–OA (102% and 37.7 MJ m^{-3}). As discussed above (*vide supra*), the superior mechanical properties of $AAPVA_x$–OA are because of the sheath–core structure in $AAPVA_x$–OA induced by the soaking treatment. The octyl enamine-enriched outer sheath is much stiffer and provides high strength and Young's modulus, while the core is unreacted soft $AAPVA_x$ and offers high ductility to $AAPVA_x$–OA. In short, here the soaking strategy creates the heterogeneous gradient structure in $AAPVA_x$–OA, which allows the strengthening and toughening of the resultant polymers.

Based on the above analysis, we establish a mechanical failure model to describe the toughening mechanism, as shown in Fig. 3d. In the tensile test, the deformation process can be divided into three stages with the increase of an applied strain. In the initial tension, both the soft layer ($AAPVA_x$) and the hard layer (the octyl enamine-enriched outer sheath) would undergo elastic deformation (stage 1). With the increase of the applied strain and corresponding higher stress, the elastic plastic stage would be reached, in which the soft layer would first start plastic deformation, while the hard layer would remain elastic. The contraction speed of the soft layer in the transverse direction would be faster than that of the hard layer. The deformation of soft $AAPVA_x$ can absorb a lot of energy, and can also prevent the generation of microcracks (stage 2). When the hard structure layer begins to deform plastically and reaches the plastic stage, the hard layer in the polymer film would shrink laterally faster than the soft layer (stage 3). It is well known that the top layer of $AAPVA_x$–OA has a low strain hardening rate due to the octyl enamine-enriched, and usually begins to deform and neck locally shortly after yielding. The soft layer of acetoacetylated polyvinyl alcohol has high strain hardening ability, which can perfectly support the unstable hard layer. Finally, once the external tensile load is high enough and the strain extends to the fracture strain, the mechanical failure of the film would occur. Therefore, the tensile properties of the soaking $AAPVA_x$–OA films can be said to be the optimization of elasticity under small deformation and energy dissipation under large strain. We envision that this soaking strategy can be implemented in other cases as well.

In addition, even with a gradient structure, the $AAPVA_{40}$–OA film is transparent with transmissivity exceeding 88% at 400–800 nm, measured using a ultraviolet-visible spectrometer (UV-vis) (Fig. 3e). The $AAPVA_{40}$–OA film is tailorable and can be cut into different shapes including rectangle, circle, dragonfly, and others (Fig. 3f). When it was cut into a strip with a dimension of 10 cm×1 cm (length and width), the $AAPVA_{40}$–OA strip can lift up a barrel of *ca.* 10 kg water, exhibiting excellent strength and toughness in the daily-life application scenario (Fig. 3g). In stark contrast, $AAPVA_{40}$–JOA is fragile and can easily break apart upon external stress. These visual illustrations vividly demonstrate the integration of high ductility and strength into $AAPVA_{40}$–OA.

3.3. Shape deformation of $AAPVA_x$–OA films

Having established the structural characteristics and mechanical properties of $AAPVA_x$–OA, we found that the treated area of $AAPVA_{40}$ with OA became hydrophobic due to the incorporation of octyl groups. First, the hydrophilicity of $AAPVA_{40}$ and $AAPVA_{40}$–OA was investigated by immersing the samples in water and then observing their swelling ratio. As shown in Fig. S6a (ESI†), after being immersed in water for 1 h, $AAPVA_{40}$

expands largely while $AAPVA_{40}$–OA remains almost the same. With a prolonged immersion time, $AAPVA_{40}$ initially shows a very rapid increase in the swelling ratio, and reaches a value of 1200% after 12 h followed by getting into a plateau (Fig. S6b, ESI†). In stark contrast, the swelling ratio of $AAPVA_{40}$–OA remains low to 35% even after 72 h of the immersion time in water (Fig. S6b, ESI†). The results strongly support that the introduction of octyl groups on the outer sheath of $AAPVA_{40}$–OA endows it with the hydrophobic nature, which is a critical feature for polymers to function stably even in high humid or rainy weather.

Leveraging the different affinities of the OA-treated (hydrophobic) or untreated (hydrophilic) areas toward water and the heterogeneous structure, created by the soaking treatment, we envision that $AAPVA_x$–OA can be configured into different shapes in the presence of water by manipulation of the soaking methods. First, we tested our hypothesis through synthesizing the bi-layered $AAPVA_{40}$–OA film by soaking one side of $AAPVA_{40}$ in the octylamine-toluene solution. In this method, the $AAPVA_{40}$ film is contacted with octylamine-toluene solution on one side, the amine group reacts with acetoacetyl group rapidly, and the patterned side of the film is asymmetrically locked by greatly increasing the top surface modulus, and the film would bend to the pattern-less side. Later, due to the unmatched expansion ability of the film in water, the curved structure would bend to the pattern side, thus forming a layer structure film with asymmetric swelling characteristics. The mismatch of swelling capacity between the two sides would lead to deformation. The pattern-less surface with faster and greater swelling capacity is the driving part, while the patterned surface with non-swelling is the memory part. Fig. 4a shows a schematic diagram of the mechanism of shape deformation induced by water swelling. The rectangular film sheet is fixed into a temporary tubular structure towards the memory side through octylamine. When it is placed in water, due to the unmatched swelling capacity of the water, the hydrogel first

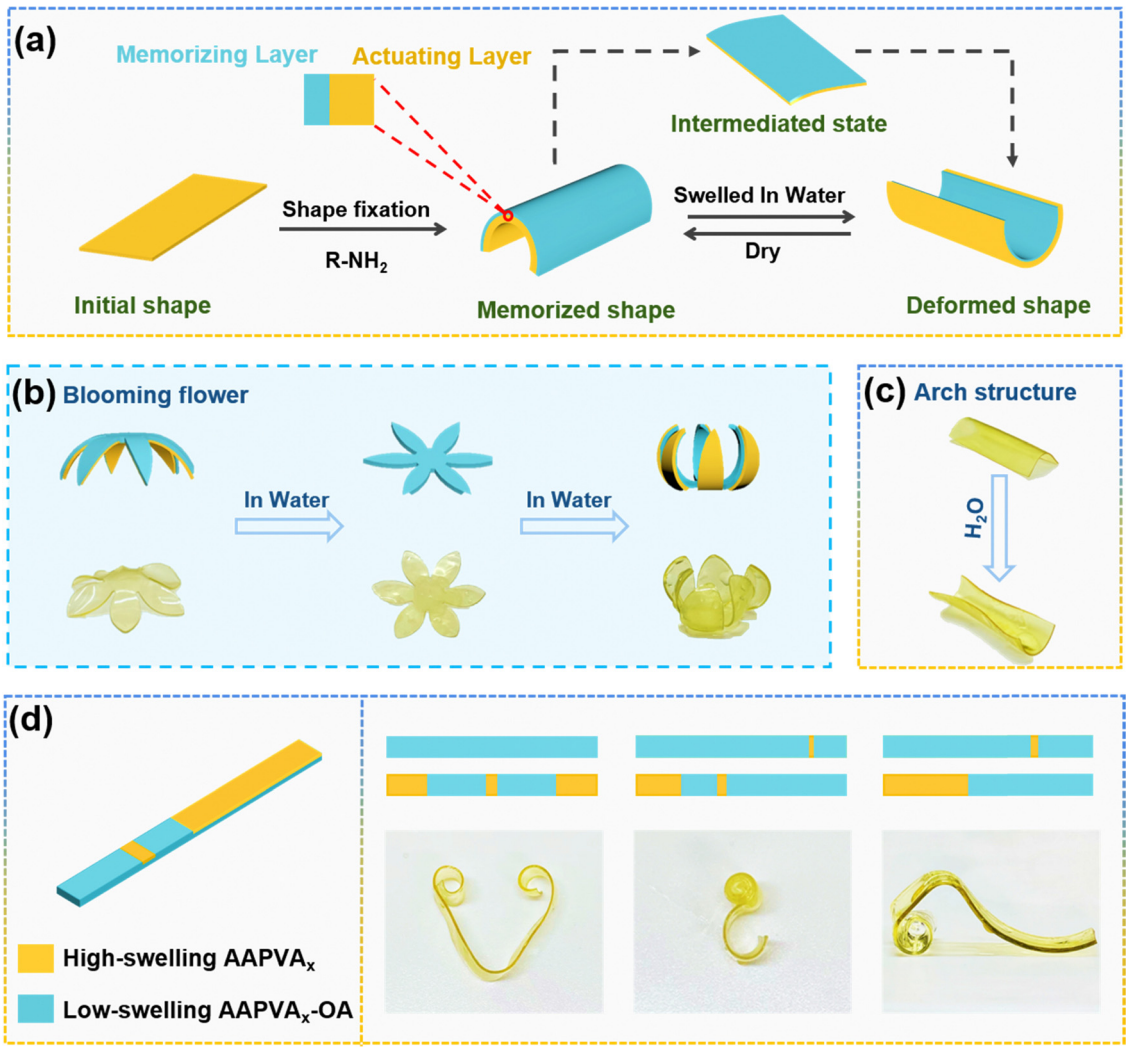

Fig. 4 (a) Schematics of the shape deformation mechanism of a bilayer film strip. 3D shape transition images of (b) flower and (c) rectangle shaped film sheets. Scale bar: 2 cm. (d) Various deformation of films with heart, hook and slide by purposefully controlling the swelling or non-swelling region, respectively.

unfolds to form a flat intermediate state, and then bends towards the pattern side due to the swelling of the actuating layer. Because the bending is caused by the swelling mismatch between the high swelling area and the non-swelling area, the deformation of the film is completely reversible. Based on this principle, temporary shapes can be manipulated through shape memory behavior, and various temporary anisotropic structures can be obtained through water driven bilayer films, thus producing different reversible shape deformation properties. For example, when the film is customized to a flower shape, the modulus difference caused by the rapid reaction of the amino group and β-dicarbonyl make the petals bend to the lower side (memory side) and be fixed first. After soaking in water, the petals first become flat, and then bend to the upper side (actuation side) to form a blooming flower (Fig. 4b). Rectangular film sheets also show similar actuation behavior (Fig. 4c). Therefore, a series of swelling or non-welling shape memory structures can be constructed by using a simple water induced shape memory function. Once the solvent is completely volatilized naturally, it would return to its original shape.

By taking advantage of the asymmetric swelling characteristics of layer structure films, complex 3D deformation can be achieved by controlling the area or shape of the memory layer or the driver layer. With the help of kirigami,[33,34] it is possible to selectively control the swelling or non-swelling of specific areas of the film to achieve complex shape transformation. As shown in Fig. 4d, we prepared a strip shaped film sheet. The middle area and two end areas were painted by high swelling $AAPVA_{40}$ structures, while the rest were painted by non-swelling $AAPVA_{40}$–OA, and then they are immersed in water. Because of the swelling of $AAPVA_{40}$, the bending stress is concentrated in the middle part and both sides, resulting in the film forming a heart shape from the strip. Similarly, by controlling the position and length ratio of the patterned surface of the film, more complex 3D shapes can be obtained in the same way, such as forming a hook like configuration, children's slide, *etc.* In addition to the above configurations, other deformable structures can also be easily programmed by using the same method. For example, hand actuators can simulate the motion behavior of various gestures. At present, we have achieved gestures such as ''good'' (Fig. S7, ESI†). We also expect that through a more complex design, the actuator can also implement more gestures to handle more complex scenes. These results indicate that $AAPVA_x$–OA prepared using the soaking strategy can broaden the range of functional polymeric materials with flexibility and versatility from shape memory to flexible actuation, and has a broad application prospect in shape memory, actuator and biomimetics applications.

4. Conclusions

In summary, we demonstrated a manufacturing method, structural characterization and practical applications which indicate that the $AAPVA_x$–OA film prepared using a soaking strategy can combine high strength and great ductility. Detailed structural characterization and comprehensive analysis fully show that its mechanical properties are much better than those of the $AAPVA_x$–JOA films synthesized using a solution blending strategy, which is mainly attributed to the strong synergistic effect of the ''soft core and hard sheath'' layer structure and hydrogen bonds at the molecular level. Because the preparation process is very simple, the soaking strategy is feasible and simple for large-scale production. In addition, depending on the structural design of an ''internal soft and external hard'' model and the difference between the internal and external hydrophobic properties, different 2D/3D shapes are also processed, which can quickly respond to solvent water and deform. We believe that this kind of film with a unique internal soft and external hard layer structure designed based on the soaking strategy can not only provide a reference for the development of polymeric materials with high mechanical strength and toughness, but also broaden the application of high-performance materials in protective coatings, flexible electronic products and intelligent actuators.

Author contributions

Xiaomin Chen completed the experiment and wrote the original draft. Youwei Ma helped with the investigation and formal analysis. Yuhong Qiao, Wenyao Guo, Jinchen Fan and Zixing Shi advised and corrected the manuscript. All authors gave approval to the final version of the manuscript.

Conflicts of interest

The authors declare no competing financial interest.

Acknowledgements

The authors thank the National Nature Science Foundation of China (51873104, 51903153, and 52073171) and the China Postdoctoral Science Foundation (2018M640382) for their financial support. This work was also funded by Science and Technology Commission of Shanghai Municipality (19DZ2271100).

Notes and references

1 K. Gong, L. Hou and P. Wu, *Adv. Mater.*, 2022, **34**, 2201065.
2 F. Barthelat, Z. Yin and M. J. Buehler, *Nat. Rev. Mater.*, 2016, **1**, 16007.
3 R. O. Ritchie, *Nat. Mater.*, 2011, **10**, 817–822.
4 A. Eckert, T. Rudolph, J. Guo, T. Mang and A. Walther, *Adv. Mater.*, 2018, **30**, e1802477.
5 J. Wei, S. Jia, C. Ma, J. Guan, C. Yan, L. Zhao and Z. Shao, *Chem. Eng. J.*, 2023, **451**, 138565.
6 A. Eckert, T. Rudolph, J. Guo, T. Mang and A. Walther, *Adv. Mater.*, 2018, **30**, 1802477.
7 H. D. Espinosa, J. E. Rim, F. Barthelat and M. J. Buehler, *Prog. Mater. Sci.*, 2009, **54**, 1059–1100.

8 J. Cao, Z. Zhou, Q. Song, K. Chen, G. Su, T. Zhou, Z. Zheng, C. Lu and X. Zhang, *ACS Nano*, 2020, **14**, 7055–7065.
9 U. G. Wegst, *J. Mech. Behav. Biomed. Mater.*, 2011, **4**, 744–755.
10 Z. Li, C. Chen, R. Mi, W. Gan, J. Dai, M. Jiao, H. Xie, Y. Yao, S. Xiao and L. Hu, *Adv. Mater.*, 2020, **32**, e1906308.
11 U. G. Wegst, H. Bai, E. Saiz, A. P. Tomsia and R. O. Ritchie, *Nat. Mater.*, 2015, **14**, 23–36.
12 S. Nikolov, M. Petrov, L. Lymperakis, M. Friak, C. Sachs, H. O. Fabritius, D. Raabe and J. Neugebauer, *Adv. Mater.*, 2010, **22**, 519–526.
13 J. Wu, Z. Qin, L. Qu, H. Zhang, F. Deng and M. Guo, *Acta Biomater.*, 2019, **88**, 102–110.
14 P. Song, Z. Xu, M. S. Dargusch, Z.-G. Chen, H. Wang and Q. Guo, *Adv. Mater.*, 2017, **29**, 1704661.
15 X. Fang, Y. Qing, Y. Lou, X. Gao, H. Wang, X. Wang, Y. Li, Y. Qin and J. Sun, *ACS Mater. Lett.*, 2022, **4**, 1132–1138.
16 H. Liu, H. Yang, K. Zhu, F. Peng, L. Guo and H. Qi, *Mater. Horiz.*, 2022, **9**, 815–824.
17 L. Rong, H. Liu, B. Wang, Z. Mao, H. Xu, L. Zhang, Y. Zhong, J. Yuan and X. Sui, *ACS Sustainable Chem. Eng.*, 2018, **6**, 9028–9036.
18 L. Rong, H. Liu, B. Wang, Z. Mao, H. Xu, L. Zhang, Y. Zhong, X. Feng and X. Sui, *Carbohydr. Polym.*, 2019, **211**, 173–180.
19 Y. Ma, Z. Liu, S. Zhou, X. Jiang, Z. Shi and J. Yin, *Macromol. Rapid Commun.*, 2021, **42**, 2100394.
20 J. Bai and Z. Shi, *Macromol. Rapid Commun.*, 2022, **44**, 2200663.
21 Y. Ma, X. Jiang, J. Yin, C. Weder, J. A. Berrocal and Z. Shi, *Angew. Chem., Int. Ed.*, 2023, **62**, 202212870.
22 J. Tie, L. Rong, H. Liu, B. Wang, Z. Mao, L. Zhang, Y. Zhong, X. Feng, X. Sui and H. Xu, *Polym. Chem.*, 2020, **11**, 1327–1336.
23 S. Zhou, J. Bai, T. Li, X. Gao, R. Xu and Z. Shi, *ACS Appl. Mater. Interfaces*, 2022, **14**, 2082–2091.
24 G. Guo, Y. Chen, X. Liu, D. Y. Zhu, B. Zhang, N. Lin and L. Gao, *J. Mater. Chem. B*, 2018, **6**, 8043–8054.
25 X. Zhou, C. Li, L. Zhu and X. Zhou, *Chem. Commun.*, 2020, **56**, 13731–13747.
26 T. Zhao, G. Wang, D. Hao, L. Chen, K. Liu and M. Liu, *Adv. Funct. Mater.*, 2018, **28**, 1800793.
27 H. Feng, Y. Ma, Z. Zhang, S. Yang, Z. Ma, Y. Zhang, S. Ma, B. Yu, M. Cai, X. Pei and F. Zhou, *Adv. Funct. Mater.*, 2022, **32**, 2111278.
28 L. Jing, H. Li, R. Y. Tay, B. Sun, S. H. Tsang, O. Cometto, J. Lin, E. H. T. Teo and A. I. Y. Tok, *ACS Nano*, 2017, **11**, 3742–3751.
29 H. Feng, J. Zhang, W. Yang, Y. Ma, R. Wang, S. Ma, M. Cai, B. Yu and F. Zhou, *ACS Appl. Mater. Interfaces*, 2021, **13**, 50505–50515.
30 S. Wan, S. Fang, L. Jiang, Q. Cheng and R. H. Baughman, *Adv. Mater.*, 2018, **30**, e1802733.
31 J. Xu, X. Wang, X. Zhang, Y. Zhang, Z. Yang, S. Li, L. Tao, Q. Wang and T. Wang, *Chem. Eng. J.*, 2023, **451**, 138673.
32 L. Li, L. Rong, Z. Xu, B. Wang, X. Feng, Z. Mao, H. Xu, J. Yuan, S. Liu and X. Sui, *Carbohydr. Polym.*, 2020, **237**, 116133.
33 X. P. Hao, Z. Xu, C. Y. Li, W. Hong, Q. Zheng and Z. L. Wu, *Adv. Mater.*, 2020, **32**, e2000781.
34 C. Y. Li, X. P. Hao, S. Y. Zheng, W. Hong, Q. Zheng and Z. L. Wu, *Adv. Intell. Syst.*, 2019, **1**, 1900055.